Accepted Manuscript

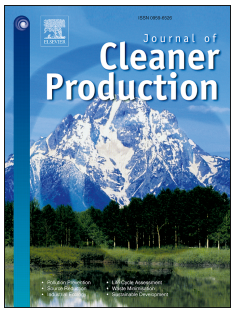

Cost effective thermoelectric composites from recycled carbon fibre: From waste to energy

Priyanka R. Jagadish, Mohammad Khalid, Lau Phei Li, Mohammad Taghi Hajibeigy, Nowshad Amin, Rashmi Walvekar, Andy Chan

PII: S0959-6526(18)31591-9

DOI: 10.1016/j.jclepro.2018.05.238

Reference: JCLP 13095

To appear in: *Journal of Cleaner Production*

Received Date: 26 March 2018

Revised Date: 14 May 2018

Accepted Date: 28 May 2018

Please cite this article as: Jagadish PR, Khalid M, Li LP, Hajibeigy MT, Amin N, Walvekar R, Chan A, Cost effective thermoelectric composites from recycled carbon fibre: From waste to energy, *Journal of Cleaner Production* (2018), doi: 10.1016/j.jclepro.2018.05.238.

Cost Effective Thermoelectric Composites From Recycled Carbon Fibre: From Waste to Energy

Priyanka R. Jagadish[1,2*], Mohammad Khalid[2*], Lau Phei Li[1], Mohammad Taghi Hajibeigy[3], Nowshad Amin[4,5], Rashmi Walvekar[3], Andy Chan[6]

[1]Department of Chemical and Environmental Engineering, Faculty of Engineering, The University of Nottingham Malaysia Campus, 43500, Semenyih, Selangor, Malaysia
[2] Graphene & Advanced 2D Materials Research Group (GAMRG), School of Science and Technology Sunway University, No. 5, Jalan Universiti, 47500 Bandar Sunway, Selangor Darul Ehsan, Malaysia
[3]School of Engineering, Taylor's University, No. 1 Jalan Taylor's, 47500 Subang Jaya, Selangor Darul Ehsan
Malaysia
[4]Department of Electrical, Electronic and Systems Engineering, Faculty of Engineering and Built Environment, The National University of Malaysia, 43600 Bangi, Selangor, Malaysia
[5]Institute of Sustainable Energy, Universiti Tenaga Nasional, Jalan IKRAM-UNITEN, 43000 Kajang, Selangor, Malaysia
[6]Department of Civil Engineering, Faculty of Engineering, The University of Nottingham Malaysia Campus, 43500 Semenyih, Selangor, Malaysia

Corresponding Authors: khalids@sunway.edu.my
priyankajagadish@yahoo.com

Abstract

Within the framework of recycling and reusing carbon fibre, this study focused on the fabrication of a thermoelectric composite encompassing recycled carbon fibre and two thermoelectric fillers (i) bismuth telluride and (ii) bismuth sulphide. This study investigated the effect of the concentration of bismuth telluride and bismuth sulphide fillers respectively on the thermoelectric, morphology, structural and thermal stability of the recycled carbon fibre thermoelectric composites. The optimum thermoelectric filler concentration is 45 wt% for both fillers, which resulted in a power factor of $0.194 \pm 9.70\times10^{-3}$ $\mu WK^{-2}m^{-1}$ and $0.0941 \pm 4.71\times10^{-3}$ $\mu WK^{-2}m^{-1}$ for recycled carbon fibre-bismuth telluride and recycled carbon fibre-bismuth sulphide composites respectively. This study exhibited the energy harvesting

capabilities of recycled carbon fibre composites from low grade waste heat when coated with thermoelectric materials.

Keywords: recycled carbon fibre, thermoelectric composites; bismuth telluride, bismuth sulphide; energy.

1. Introduction

Carbon fibre-reinforced composites are now steadily being preferred in the automotive, aerospace and industrial applications due to its lightweight, flexibility and robust mechanical properties (Shuaib & Mativenga, 2016; Marsh, 2014; Timmis et al., 2015; Tian et al., 2017). This increasing preference has led to approximately 3000 tonnes of carbon fibre scrap composites produced by United States of America (USA) and Europe annually (McConnell, 2010). The Landfill Directive (1999/31/EC) has enforced environmental legislation that compels industry stakeholders to explore alternative disposal methods for these carbon fibre-reinforced scrap instead of conventional incineration and landfill disposal (Marsh, 2009; Howarth et al., 2014).

Recycled carbon fibre (RCF) has been primarily explored for its mechanical properties in structural applications (Cholake et al., 2016; Li et al. , 2016; Feng et al. , 2013), however recycling leads to a slight decrease in tensile strength properties which makes it challenging to be used for structural purposes currently. RCF cannot be used as a direct substitute of virgin carbon fibre in critical structural applications, as it would not have the same strength and rigidity (Li et al., 2016). Hence, different routes to use RCF should be explored to close the recycling loop in which mechanical properties are not as vital. One such application is utilising RCF in the field of thermoelectricity. Thermoelectricity is the conversion of widely available thermal energy (i.e. waste heat from refrigerators, air-conditioners, exhaust pipes of vehicles, electronic gadgets) into usable electricity (Fernández-Yáñez et al., 2018; Kishita et al., 2016).

Though recycling leads to reduction of mechanical properties, the electrically conductive nature of carbon fibres are preserved despite recycling (Wong et al., 2010). Carbon fibre is an electrical conductor that is weakly thermoelectric, has enabled it to be integrated into polymer-matrix composites and also cement composites for thermoelectric and heating applications as fillers (Wang et al., 2014; Tsukamoto et al., 1989; Hambach et al., 2016). RCF has previously been explored by the authors as a flexible substrate in electrodeposited bismuth telluride (Bi_2Te_3) thin films and exhibited positive thermoelectric capabilities (Pang et al., 2012; Jagadish et al., 2016; Jagadish et al., 2017).

However, for practical application the thickness of thin films are just too small to sustain a substantial temperature difference for thermoelectric energy harvesting. Moreover for large-scale conversion of thermal to electrical energy, thin film techniques require high cost of processing, special infrastructure, time consuming and are energy intensive. In addition to that, the previously used electrodeposition technique also results in toxic solvent disposal issues as most electrolytes used are strongly acidic such as hydrochloric and nitric acids.

Therefore, in order to overcome the shortcomings of the previous technique, this research work focuses on the development of a low-cost effective RCF polymer thermoelectric composite using a combination of hot compression and brushing technique. To the best of the author's knowledge, no prior work has been done on the hybrid RCF-inorganic thermoelectric filler polymer thermoelectric composite. In this study, the inorganic thermoelectric filler chosen is n-type bismuth telluride (Bi_2Te_3) as it has the highest reported value of ZT≈ 1.4 at a room-temperature range of 200–400 K which is suitable for portable power generators (Venkatasubramanian et al., 2001; Kusagaya and Takashiri, 2015).

Although telluride based thermoelectric materials especially Bi_2Te_3 have high figure of merit (ZT) values at approximately 1.2 (Venkatasubramanian et al., 2001; Wang et al., 2015)

showing superior thermoelectric properties and hold dominant market share in thermoelectric industry, it is imperative to develop alternative materials because of the rare nature of availability and toxicity of tellurium (Zhao et al., 2008). Bi_2S_3 has recently acquired much attention due to its environmentally friendly nature and its potential application in the thermoelectric field (Yu et al., 2011; Wong et al., 2016). Bismuth sulphide (Bi_2S_3) is promising in this respect because of its abundance, high Seebeck coefficient and low thermal conductivity. Thus, the second part of this study also investigated the thermoelectric properties of Bi_2S_3 coated RCF composite.

This work focused on the optimisation of the concentration of thermoelectric fillers and its subsequent effect on the thermoelectric properties (i.e. Seebeck coefficient, electrical resistivity and power factor) for both Bi_2Te_3 and Bi_2S_3. The morphological, structural and also the thermal stability of the RCF composites filled with Bi_2Te_3 and Bi_2S_3 were also demonstrated in this work.

2. Material and Methods

2.1. Materials

The inorganic thermoelectric fillers used are bismuth (III) telluride and bismuth (III) sulphide powders. The bismuth (III) telluride powders with a relative density of 7.6 g/cm^3 and purity of 99.99% was purchased from Sigma Aldrich Sdn. Bhd. Bismuth (III) sulphide powders with a relative density of 7.7 g/cm^3 and purity of 99% was purchased from Sigma Aldrich Sdn. Bhd. A water-based formaldehyde-free cross-linked acrylate binding polymer, Acrodur DS 3530 was supplied by BASF Malaysia Sdn. Bhd. The recycled carbon fibres used in this experiment are recycled Toray T600 carbon fibre recovered via fluidised bed process supplied by Recycled Carbon Fibre Limited (RCF) Coseley, UK.

2.2. Thermoelectric Composite Fabrication

2.2.1 RCF Composite

Layers of randomly oriented RCF were placed in a binder-water suspension with a 1: 10 (volume ratio). The RCF was soaked in the suspension for approximately 15 minutes. The soaked RCF was sandwiched between two metal plates that were covered with laboratory wipes on the top and bottom plate to remove the residual water. The top metal plate was then manually subjected to a brick load of 10 kg to produce a uniform RCF composite with a thickness of 1 mm. The laboratory wipes were replaced with new ones once it was wet and the RCF were subjected to the same load for approximately three times until it was dried. The dried RCF with an applied top load of 5 kg was then placed in a Memmert oven at 200 °C for 1 hour for moisture evaporation and also curing and formation of the RCF composite.

2.2.2 Thermoelectric Filler Coating on RCF composite

Two thermoelectric fillers are used in this work, namely Bi_2Te_3 and Bi_2S_3 particles. The thermoelectric filler particles are mixed with ethylene glycol and Acrodur DS 3530 binder and are subjected to ultrasonication for one hour, this ultrasonicated solution will thereafter be referred to as thermoelectric filler coating. The thermoelectric filler coating is then applied to the surface of the RCF composite using a brushing technique (using paint brush). The coated RCF composite is then placed into the oven at 200 °C for 1 hour. The weight percent of both thermoelectric fillers were varied from 15 to 60 weight percent (wt%) within the composite.

2.3. Characterization

2.3.1. Seebeck coefficient

The Seebeck coefficient was measured using an in-house measurement system (see **Figure S.1** in Supplementary data).

The Seebeck coefficient is calculated using the formula shown in Eq (1):

$$\alpha = \frac{\Delta V}{\Delta T} = \frac{V_H - V_C}{T_H - T_C} \qquad (1)$$

ΔV in millivolts is the open circuit potential difference (V_{OC}) generated between V_H, the potential at the hot side and V_C, the potential at cold side, ΔT in Kelvin is the temperature induced between the T_H, temperature on the hot side and T_c, temperature on the cold side. The test was conducted with an average measuring temperature of 40 °C on the hot side and cold side subjected to room temperature. Whereby, α is the combined measured value of the Seebeck coefficient of copper (α_{CU}) and RCF thermoelectric composite (α_{CF}), therefore the Seebeck coefficient of RCF thermoelectric composite is given by Eq (2).

$$\alpha_{CF} = \alpha_{Cu} - \alpha \qquad (2)$$

The Seebeck coefficients of the carbon fibres were calculated using Eq (2) by taking an average of all six readings.

2.3.2. Hall Effect measurement

The electrical parameters such as electrical resistivity, carrier concentration and carrier mobility was measured using a Hall Effect measurement system, HMS ECOPIA 3000 with a magnetic field 0.57T and probe current of 15mA for all samples.

2.3.3. Power Factor Calculation

The performance/efficiency of a thermoelectric composite is given by the power factor (PF) with the formula shown in Eq (3) (Kim and Oh, 2009).

$$PF = \frac{\alpha^2}{\rho} \qquad (3)$$

PF is calculated based on measured values of both α and ρ.

2.3.3. Phase analysis

The phase structure and crystallinity property analysis of the RCF thermoelectric composites was determined by X-ray powder diffraction (XRD) (Cu-Kα, Bruker D8 Advance) operating at 40kV and 40 mA. XRD patterns were recorded in the 2θ range from 10 to 80° with a step size of 0.025° using Cu Kα radiation wavelength of 1.540 Å.

Crystallite size (D) can be calculated using the Scherrer equation as shown in Eq (4):

$$D = \frac{0.9\lambda}{\beta cos\theta} \qquad (4) \qquad \text{(Hasan and Shallal, 2014)}$$

Where θ is the Bragg diffraction angle, λ is the wavelength of x-ray (1.540 Å), β is the full width at half maximum (FWHM) of the main peak in the XRD pattern.

The microstrain (ε) of the thermoelectric composites are calculated using the formula in Eq (5):

$$\varepsilon = \frac{\beta}{4\tan\theta} \qquad (5) \qquad \text{(Yücel and Yücel, 2017a)}$$

Dislocation density (δ) is defined as the length of dislocation lines per unit volume of the crystal space is calculated using Eq (6):

$$\delta = \frac{1}{D^2} \qquad (6) \qquad \text{(Yücel and Yücel, 2017b)}$$

2.3.4. Field Emission Scanning Electron Microscope (FESEM) and Energy Dispersive X-Ray (EDX) Analysis

The RCF thermoelectric composites were cut into 1 cm x 1 cm and placed onto a double-sided sticky tape that was positioned on sample pins before being placed into the FESEM machine. The FESEM images were taken using the FEI Quanta 400 to obtain the morphological structure of the composites. The EDX analysis was carried out to determine the percentage distribution of bismuth, tellurium and sulphur in the composites.

2.3.5. Thermogravimetric Analysis (TGA)

Thermal degradation and stability of the RCF thermoelectric composites were measured using a thermogravimetric analyser (Perkin Elmer STA 6000). A sample of approximately 10-15 mg in weight was placed in an open alumina pan under an air flow rate of 20 ml/min and heated from ambient 30 °C to 900 °C at a heating rate of 10 °C/min. The onset degradation temperature (T_{onset}) is defined as the temperature at 5% weight loss. Maximum degradation temperature (T_{max}) is defined as temperature at which the thermoelectric composite losses its maximum weight, that is identified by the peak of derivative (dW/dT) curve. These temperatures were used to indicate the thermal degradation and stability of the RCF thermoelectric composites.

3. Results and discussions

3.1. Thermoelectric properties of RCF composites coated with Bi_2Te_3 and Bi_2S_3

Seebeck coefficient, electrical resistivity and power factor of RCF composites coated with different weight concentrations of Bi_2Te_3 and Bi_2S_3 are shown in **Figure 1** to **Figure 4**. Based on **Figure 1**, it was observed that RCF composites exhibited weakly p-type thermoelectric nature with a Seebeck coefficient of +4.52 ± 0.226 µV/K. Upon the incorporation of Bi_2Te_3 and Bi_2S_3 coating on the surface of RCF composite, the thermoelectric nature of the RCF composite shifts from p-type to n-type as shown in **Figure 1**. All Bi_2Te_3 and Bi_2S_3 coated RCF composites displayed negative Seebeck coefficients owing to the change in conductivity. This shift is because Bi_2Te_3 and Bi_2S_3 used in this study are n-type semiconductors which are electron dominant.

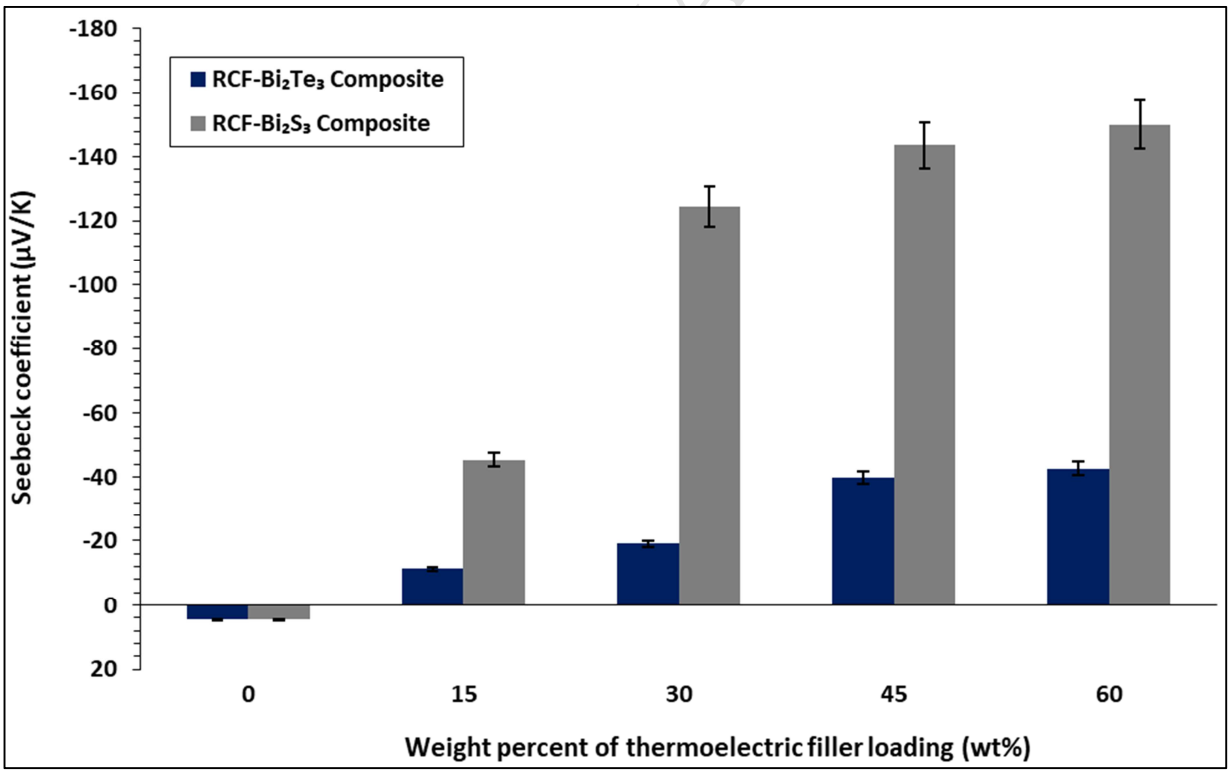

Figure 1: The effect of Bi_2Te_3 and Bi_2S_3 concentrations on the Seebeck coefficient of RCF-Bi_2Te_3 and RCF-Bi_2S_3 composites.

As both Seebeck coefficient and electrical resistivity are highly dependent on the carrier concentration, their changes can be justified by the variation in carrier concentration as shown in Eq (7) and Eq (8).

$$\rho = \frac{1}{ne\mu} \quad (7) \quad \text{(Li et al., 2011)}$$

$$\alpha = \pm\frac{k_B}{e}\left[(r+2) + \ln\frac{2(2\pi m^* k_B T)^{3/2}}{h^3 n}\right] \quad (8) \quad \text{(Li et al., 2011)}$$

Where, ρ is the electrical resistivity, n is carrier concentration, e is the electron charge (1.60×10^{-19} coulombs), μ is carrier mobility, α is the Seebeck coefficient, k_B is Boltzmann's constant, r is the scattering factor, m^* is effective mass, h is Planck constant and T is temperature.

The Seebeck coefficient of both composites was observed to increase linearly with respect to the concentration of the Bi_2Te_3 and Bi_2S_3 particles as shown in **Figure 1**. An increase in Seebeck coefficient is a result of decreased carrier concentration as deduced from Eq (8) above. The carrier concentration for RCF-Bi_2Te_3 composites decreased by approximately 62% from 1.43×10^{21} cm^{-3} (15 wt%) to 4.50×10^{20} cm^{-3} (60 wt%) and that of RCF-Bi_2S_3 composites by approximately 92% from 4.59×10^{19} cm^{-3} (15 wt%) to 3.27×10^{18} cm^{-3} (60 wt%) as shown in **Table 1**. RCF are inherently conductive due to its carbon content, thus having a higher amount of carrier concentrations. However, with the increased incorporation of semiconductors such as Bi_2Te_3 and Bi_2S_3 on RCF, the composites transition from a conductive to semi-conductive nature, suppressing the density of its carrier concentration. It is also important to emphasize that the Seebeck coefficient of RCF-Bi_2S_3 composites are higher than that of RCF-Bi_2Te_3 composites at all loadings. This is because Bi_2S_3 has intrinsic carrier concentrations around 10^{18} cm^{-3} that are two orders lower than that of Bi_2Te_3 (10^{20} cm^{-3}) (Rowe, 1995).

A similar increase in Seebeck coefficient was observed by Li et al., as the concentration of Bi_2Te_3 was increased in a high performance $(Bi_2Te_3)_x(Sb_2Te_3)_{1-x}$ bulk materials due to the large difference in electronegativity between Bi and Te atoms that suppresses the carrier concentrations (Li et al., 2011).

Table 1: Carrier concentration and carrier mobility of thermoelectric composites with respect to increasing Bi_2Te_3 and Bi_2S_3 concentrations.

Weight percent of thermoelectric filler (wt%)	Carrier concentration for RCF-Bi_2Te_3 composites (cm^{-3})	Carrier mobility for RCF-Bi_2Te_3 composites ($cm^2V^{-1}s^{-1}$)	Carrier concentration for RCF-Bi_2S_3 composites (cm^{-3})	Carrier mobility for RCF-Bi_2S_3 composites ($cm^2V^{-1}s^{-1}$)
15	1.43×10^{21}	4.62×10^{-3}	4.59×10^{19}	5.94×10^{-3}
30	9.70×10^{20}	7.31×10^{-3}	9.55×10^{18}	3.40×10^{-2}
45	6.01×10^{20}	1.27×10^{-2}	4.27×10^{18}	6.67×10^{-2}
60	4.50×10^{20}	1.49×10^{-2}	3.27×10^{18}	7.37×10^{-2}

The influence of the concentration of Bi_2Te_3 and Bi_2S_3 particles on the electrical resistivity of the composites are shown in **Figure 2**. As the changes in electrical resistivity of RCF-Bi_2Te_3 composites are not apparent in **Figure 2** due to much higher resistivity of RCF-Bi_2S_3 composites, a zoomed in-view is plotted in **Figure 3**. All RCF-Bi_2Te_3 and RCF-Bi_2S_3 composites exhibited higher electrical resistivity than that of pure RCF composites (0 wt%), attributed to the decreased carrier concentrations. Both RCF-Bi_2S_3 and RCF-Bi_2Te_3 depicted an initial increase in resistivity from 0 wt% to 15 wt% as shown in **Figure 2**, this behaviour is observed due to the presence of polymeric binder in the coating on the surface of RCF. However, a decreasing trend in the electrical resistivity was observed from 15 wt% to 45 wt% and 15 wt% to 30 wt% for RCF-Bi_2Te_3 and RCF-Bi_2S_3 composites respectively. This decreasing trend is owing to the improvement in carrier mobility by one order from 4.62×10^{-3} $cm^2V^{-1}s^{-1}$ (15 wt%) to 1.27×10^{-2} $cm^2V^{-1}s^{-1}$ (45 wt%) in RCF-Bi_2Te_3 and 5.94×10^{-3} $cm^2V^{-1}s^{-1}$ (15 wt%) to 3.40×10^{-2} $cm^2V^{-1}s^{-1}$ (30 wt%) in RCF-Bi_2S_3 respectively as shown in **Table 1**. Bi_2Te_3 and Bi_2S_3 particles acts as a bridge between the haphazardly arranged RCF strands, thus facilitating electron transport throughout the composite. Rahman et al. also

observed a similar decrease in electrical resistivity when poly(3.4-ethylenedioxythiophene)-poly(styrenesulfonate) (PEDOT: PSS) was doped with Bi_2Te_3 until a maximum of 0.8 wt% whereby beyond that there was intense dopant aggregation that resulted in increased electrical resistivity (Rahman et al., 2015). However increased loading of Bi_2Te_3 and Bi_2S_3 beyond 45 wt% and 30 wt% respectively, exhibited a detrimental effect on the electrical resistivity as shown in **Figure 2**, due to the continuous decrease in carrier concentration and only marginal improvement in carrier mobility at higher loadings.

Based on **Figure 2**, it is also observed that RCF-Bi_2S_3 displayed a higher resistivity than that of RCF-Bi_2Te_3 at all concentrations. This is due to the difference in band gap between these two semiconductors, Bi_2S_3 has a band gap of 1.3 eV (Liufu et al., 2007) whereas that of Bi_2Te_3 is at 0.17 eV (Kioupakis et al., 2010). Band gap influences the intrinsic carrier concentration and this relationship is described in Eq (9) below:

$$n_i = \sqrt{N_C N_V}\exp\left(\frac{-E_g}{2kT}\right) \quad (9)$$ (Keuch, 2015)

Where, n_i is the intrinsic carrier concentration, N_C is the effective density of states in the conduction band, N_V is the effective density of states in the valence band, E_g is the band gap, k is Boltzmann's constant and *T* is temperature. Therefore, as the band gap of Bi_2S_3 is wider than that of Bi_2Te_3, intrinsically it has fewer carrier concentrations thus rendering it more resistive.

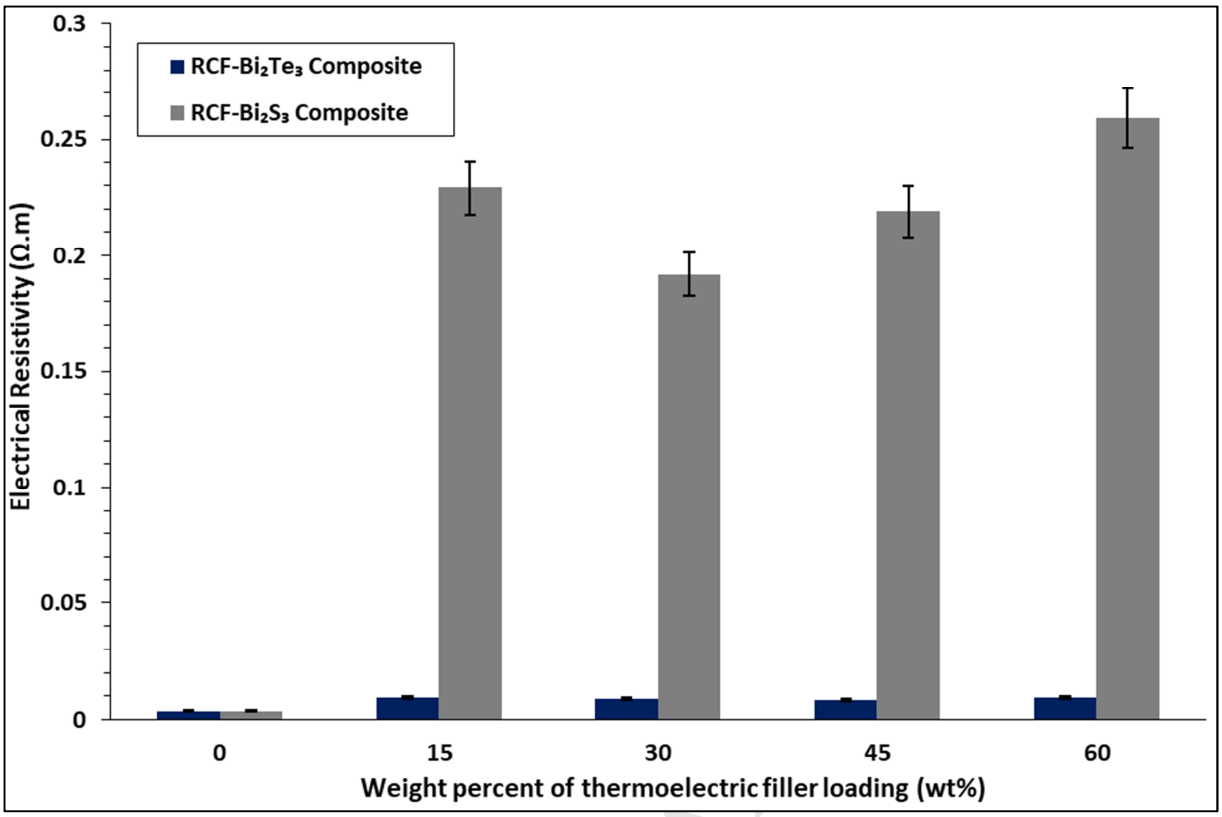

Figure 2: The effect of Bi_2Te_3 and Bi_2S_3 concentrations on the electrical resistivity of RCF-Bi_2Te_3 and RCF-Bi_2S_3 composites.

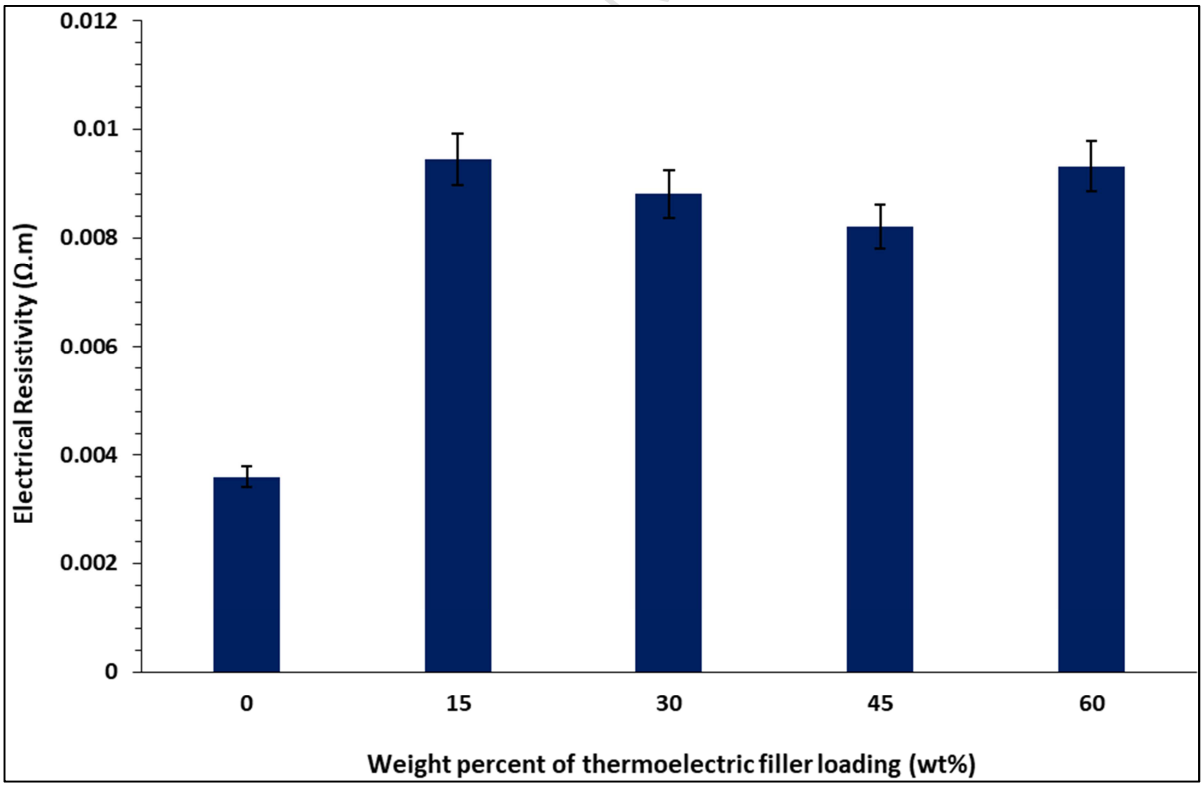

Figure 3: Zoomed in view on the electrical resistivity of RCF-Bi_2Te_3 composites with respect to varying concentrations of Bi_2Te_3.

The power factor of RCF-Bi_2Te_3 and RCF-Bi_2S_3 composites is calculated taking into consideration both Seebeck coefficient and electrical resistivity and the corresponding values is as shown in **Figure 4**. The highest power factor obtained for RCF-Bi_2Te_3 and RCF-Bi_2S_3 composites are $0.194 \pm 9.70\times10^{-3}$ $\mu WK^{-2}m^{-1}$ and $0.0941 \pm 4.71\times10^{-3}$ $\mu WK^{-2}m^{-1}$ respectively, both composites attained the highest power factor at 45 wt% of thermoelectric filler loading. The environmentally friendly RCF-Bi_2S_3 thermoelectric composite is approximately 95% lower in power factor compared to that of RCF-Bi_2Te_3 composites. The lower thermoelectric performance of RCF-Bi_2S_3 composites could be attributed to its resistivity. The highest resistivity of RCF-Bi_2S_3 composites is $0.259 \pm 1.30 \times10^{-2}$ Ω.m whereas that of RCF-Bi_2Te_3 is $9.44\times10^{-3} \pm 4.72\times10^{-4}$ Ω.m, which renders Bi_2S_3 27.4 times more resistive than Bi_2Te_3. The resistive nature of Bi_2S_3 is due to its low carrier concentrations, the lowest carrier concentration of RCF-Bi_2S_3 composite is 3.27×10^{18} cm^{-3} whereas that of RCF-Bi_2Te_3 composite is 4.50×10^{20} cm^{-3} as shown in **Table 1** which is approximately two orders lower than Bi_2Te_3. However, the naturally low carrier concentrations in Bi_2S_3 resulted in higher Seebeck coefficient of RCF-Bi_2S_3 (-150.1 ± 7.51 $\mu V/K$) composites approximately 252% higher than that of RCF-Bi_2Te_3 (-42.6 ± 2.13 $\mu V/K$) composites.

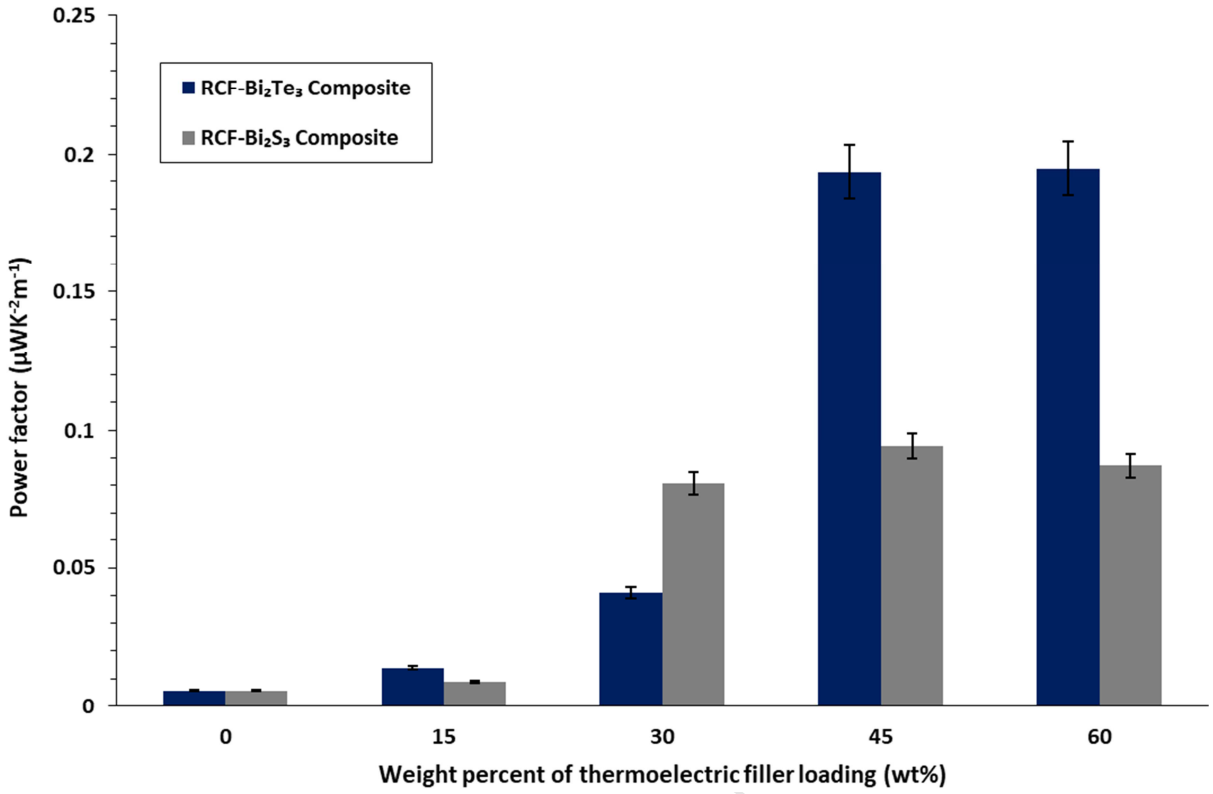

Figure 4: The effect of Bi_2Te_3 and Bi_2S_3 concentrations on the power factor of RCF-Bi_2Te_3 and RCF-Bi_2S_3 composites.

The thermoelectric properties of RCF-Bi_2S_3 can be further enhanced in future works through increase in the electronic density of states (DOS) and band engineering by doping (Yu et al., 2011;Du et al., 2014), nanostructuring (Liufu et al., 2007) and introducing sulphur vacancies (Zhao et al., 2008). Though in this study RCF-Bi_2S_3 composites exhibited lower thermoelectric performance than that of RCF-Bi_2Te_3, but with future modifications through band engineering, RCF-Bi_2S_3 composites can be a plausible non-toxic alternative to telluride based thermoelectric materials.

The current limitation of the thermoelectric composites produced in this study is its rigidity and lack of flexibility. To enable the usability of these composites on waste heat areas with different surface geometry, flexibility is a vital parameter. Flexibility as well as the electrical conductivity of these composites can be improved by employing electrically conductive

316 polymers such as polyaniline (PANI), poly (3,4-ethylenedioxythiophene)-
317 poly(styrenesulfonate) (PEDOT: PSS) and polythiopene for future works.

318 The potential application of the recycled carbon fibre thermoelectric composites fabricated in
319 this study is in the field of energy harvesting from waste heat with a minimum hot side
320 temperature of 40 °C such as that from electronic devices, glass windows in air-conditioned
321 buildings and cars and any other mild waste heat generating surface.

322 **3.2. FESEM and EDX study of RCF-Bi_2Te_3 and RCF-Bi_2S_3 composites**

323 The FESEM images were used to study the morphology of the composites. In the cross-
324 sectional view, the RCF strands are seen to be buried in the Bi_2Te_3–binder coating (see
325 **Figure S.2** in Supplementary data). All three components in the RCF-Bi_2Te_3 composite,
326 which are RCF, polymeric binder and Bi_2Te_3 powder can be clearly observed in **Figure S.3**
327 (see Supplementary data). The RCF strands are predominantly carbon, C and have 2 atomic
328 percent (at%) of oxygen, O coming from some residual epoxy from previous applications and
329 also due to some binder attaching itself on the surface of RCF as depicted in **Figure S.3 (a)**
330 (see Supplementary data). The polymeric binder used in this study was Acrodur 3530 S, a
331 dispersion of a modified polycarboxylic acid and a polyol (cross-linking agent) thus resulting
332 in elements such as C and O in its EDX as shown in **Figure S.3 (b)** (see Supplementary data)**.**
333 The EDX analysis of Bi_2Te_3 powder indicated 58.52 at.% of Te and 41.48 at.% of Bi as
334 displayed in **Figure S.3 (c)** (see Supplementary data).

335 **Figure 5** shows the effect of increasing Bi_2Te_3 concentration within the RCF-Bi_2Te_3
336 composite. At lower loadings of Bi_2Te_3 in the composite (15 wt% and 30 wt%), it can be seen
337 that there is not sufficient amount of Bi_2Te_3 particles filling up the gaps between the RCF
338 strands and having low coverage, thus leading to lower power factors. However, from 45
339 wt% onwards there seems to be sufficient Bi_2Te_3, and/no visible gaps were observed in the

FESEM image which led to saturation at 60 wt%. Thus, the values of power factors plateaued with no further increase.

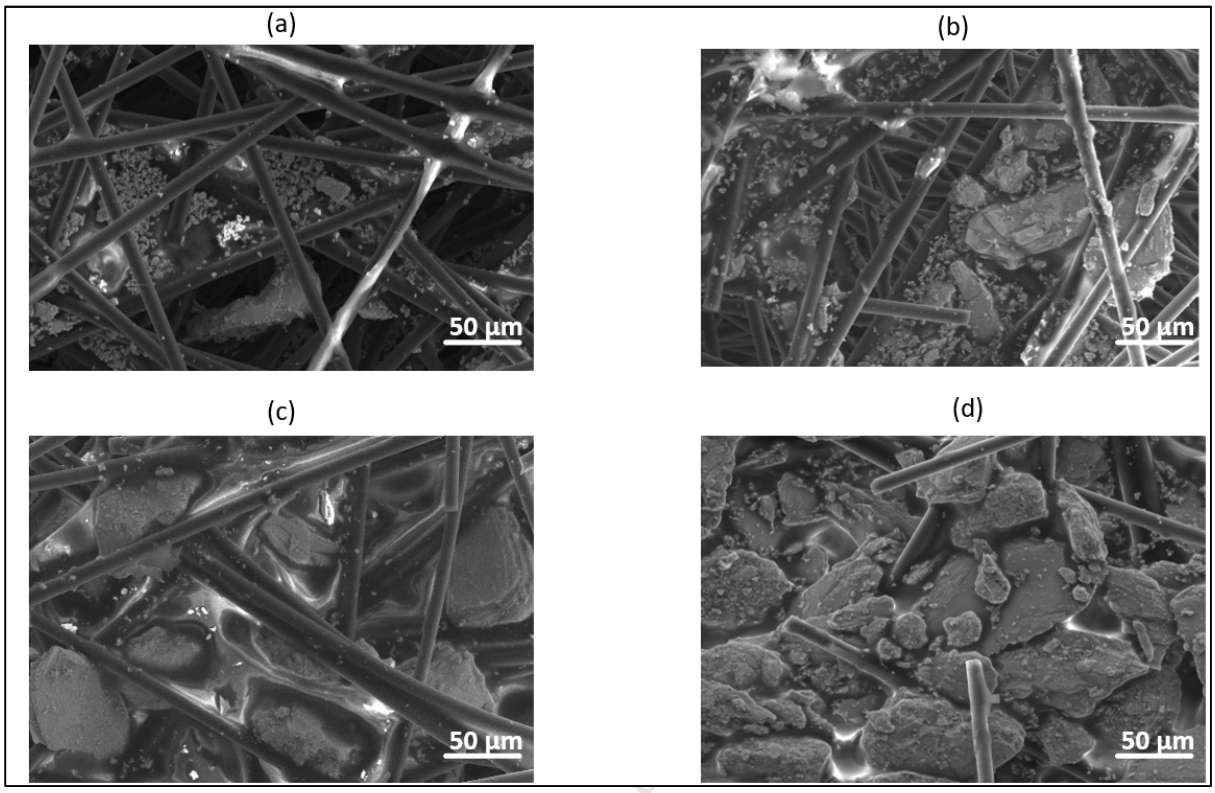

Figure 5: FESEM surface images of RCF-Bi_2Te_3 composite at (a) 15 wt% (b) 30 wt% (c) 45 wt% (d) 60 wt% of Bi_2Te_3.

A similar image of RCF being buried in Bi_2S_3 -binder coating can be seen in **Figure S.4** (see Supplementary data). The Bi_2S_3 is seen to coat each RCF strand from the cross-sectional view and subsequently filling in the gaps between the haphazardly arranged RCF similar to that of Bi_2Te_3.

Figure S.5 (see Supplementary data) shows all three components present within the RCF-Bi_2S_3 composite which are (a) RCF strands, (b) polymeric Acrodur binder 3530 S and (c) Bi_2S_3 particles. **Figure S.5 (a-c)** (see Supplementary data) also shows the corresponding EDX study of all three components present within the composite. The EDX of RCF and polymeric binder is similar to that discussed above for RCF-Bi_2Te_3 composites. The EDX of

355 Bi_2S_3 particles as shown in **Figure S.5 (c)** (see Supplementary data), indicates 61.05 at.% of S
356 and 38.95 at.% of Bi which is deviating from its stoichiometric composition of 60 at.% of S
357 and 40 at.% of Bi. The enrichment in sulphur in the stoichiometry of the as-received powders
358 may have resulted in higher electrical resistivity of the RCF-Bi_2S_3 composites.

359 Referring to **Figure 6**, it can be seen that the gap between RCF strands have been filled with
360 Bi_2S_3 particles from 30 wt% onwards which corresponds to increasing power factor values as
361 shown in **Figure 4**. At 60 wt% (see **Figure 6 (d)**), it can be seen that the RCF strands are not
362 completely embedded in the polymer-Bi_2S_3 coating when compared to **Figure 6 (a-c)**. There
363 is a separation of polymeric binder phase from the Bi_2S_3 particles perhaps owing to the high
364 loading of Bi_2S_3 particles, thus also leading to a drop in power factor as shown in **Figure 4**.

365 With optimum loading of Bi_2Te_3 and Bi_2S_3, the thermoelectric fillers acts as a bridge to fill in
366 the gaps between the RCF strands. Thus, allowing for better transport of electrons across the
367 composite which is proven by the improved carrier mobility as shown in **Table 1**.

368 Thus, it can be concluded based on surface morphology and thermoelectric properties, 45
369 wt% is the highest optimum filler concentration for both RCF-Bi_2Te_3 and RCF-Bi_2S_3
370 composite.

371

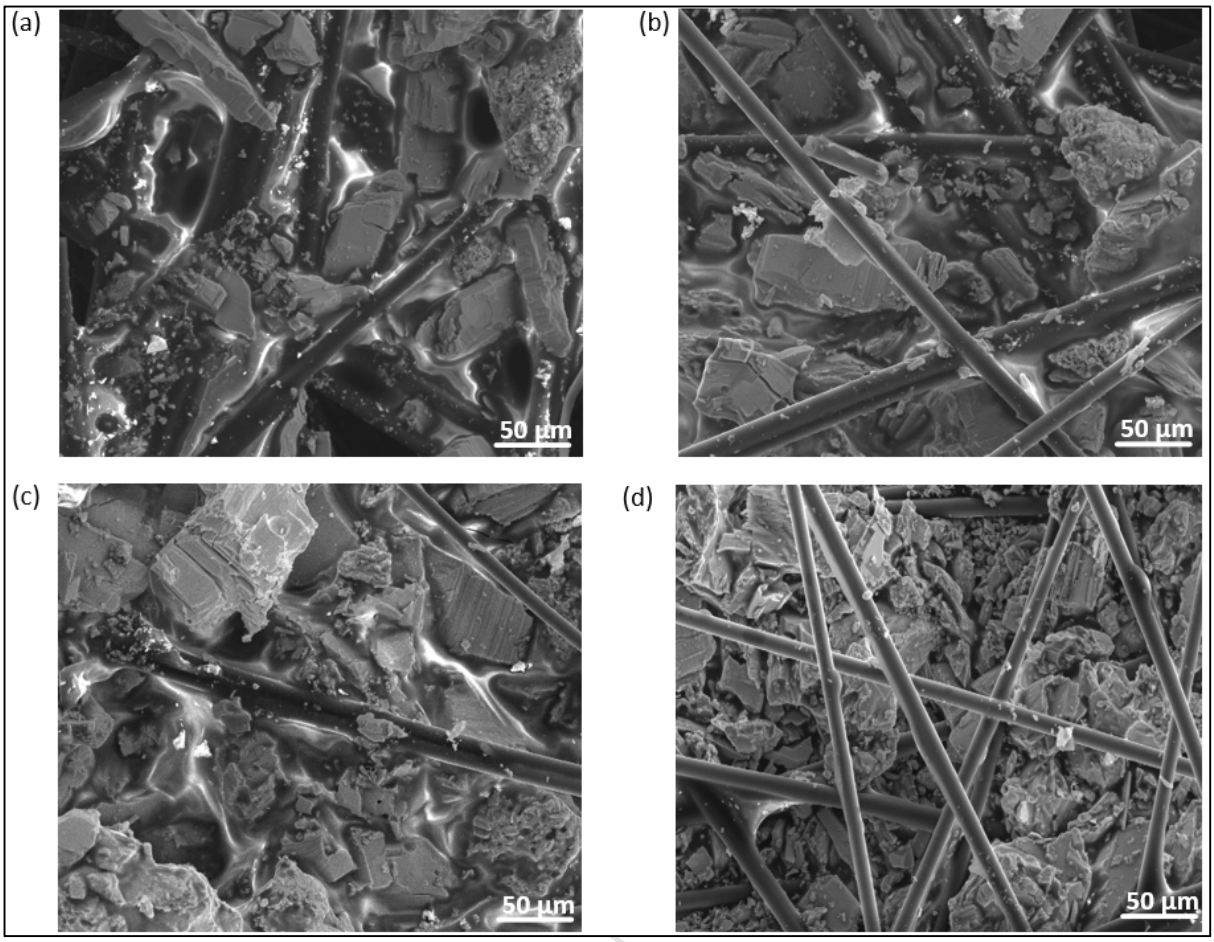

Figure 6: FESEM surface images of RCF-Bi_2S_3 composite at (a) 15 wt% (b) 30 wt% (c) 45 wt% (d) 60 wt% of Bi_2S_3.

3.3. XRD Analysis of RCF-Bi_2Te_3 and RCF-Bi_2S_3 composites

The obtained XRD patterns for RCF-Bi_2Te_3 composites from X-ray diffractometer are shown in **Figure 7**. The following 12 diffraction peaks of Bi_2Te_3 located at 2θ, 17.59°, 27.78°, 37.93°, 40.42°, 41.27°, 44.64°, 50.37°, 54.00°, 57.17°, 62.31°, 66.04° and 67.17° with orientations of (006), (015), (1010), (0111), (110), (0015), (205), (1016), (0210), (1115), (0120) and (125) were observed for all the RCF-Bi_2Te_3 composite.

At all loadings of Bi_2Te_3, all 12 diffraction peaks mentioned above are observed. These values are in good agreement with standard data of Joint Committee on Powder Diffraction Standards (PDF 00-015-0863) data and the observed peak positions are consistent with the

rhombohedral structure of Bi_2Te_3 and observed peak positions are represented by their corresponding Miller indices in the spectra. The most prominent peak is (015) was used to calculate all XRD related parameters for RCF-Bi_2Te_3 composites.

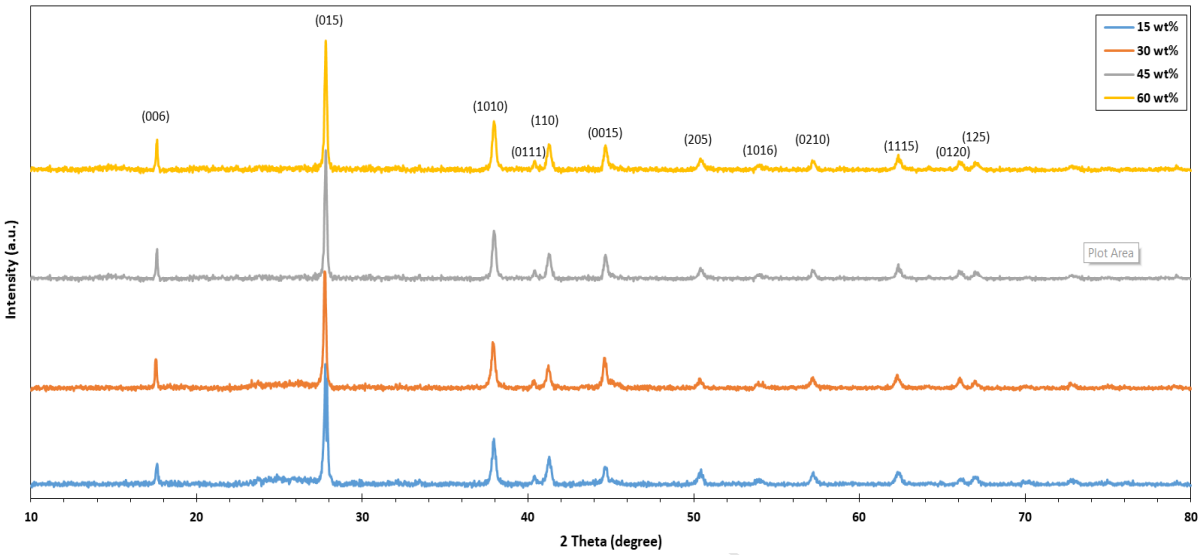

Figure 7: X-Ray diffraction patterns of RCF-Bi_2Te_3 composite at different Bi_2Te_3 concentrations.

For the RCF-Bi_2S_3 composite, the XRD spectra are as shown in **Figure 8.** The following 24 diffraction peaks of Bi_2S_3 located at 2θ, 15.75°, 17.62°, 22.43°,24.99°, 25.23°, 27.49°, 28.65°, 31.84°, 33.04°, 33.96°, 35.65°, 36.68°, 39.09°, 39.95°, 45.60°, 46.51°, 47.05°, 48.48°, 49.21°, 52.63°, 53.86°, 54.77°, 62.68° and 64.57° with orientations of (200), (201), (202),(301),(103), (210), (112), (212), (013), (303), (402), (312), (410), (411), (020), (314), (511), (600), (512), (321), (610), (611), (711) and (712) were observed for all RCF-Bi_2S_3 composite.

At all loadings of Bi_2S_3, all 24 diffraction peaks mentioned above are observed. These values are in good agreement with standard data of Joint Committee on Powder Diffraction Standards (PDF 01-074-9437) data and the observed peak positions are consistent with the orthorhombic structure of Bi_2S_3 and observed peak positions are represented by their

corresponding Miller indices in the spectra. The most prominent peak is (301) was used to calculate all XRD related parameters for RCF-Bi_2S_3 composites.

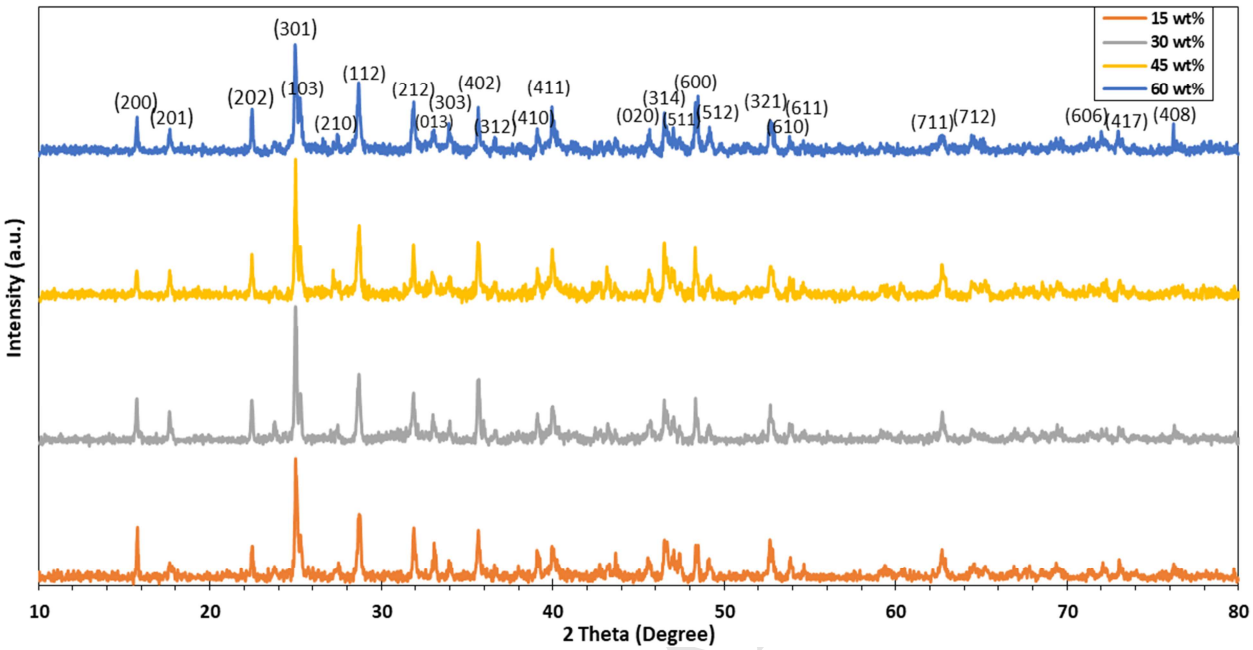

Figure 8: X-Ray diffraction patterns of RCF-Bi_2S_3 composite at different Bi_2S_3 concentrations.

With the increasing amount of Bi_2Te_3 and Bi_2S_3, there is a slight increase in crystallite size from 15 wt% to 30 wt% as shown in **Table 2** and **Table 3** respectively. However, from 30 wt% to 60 wt% the crystallite size is kept constant around 46-47 nm for RCF-Bi_2Te_3 composite and the crystallite size is kept constant around 52-53 nm from 30 wt% to 45 wt% for RCF-Bi_2S_3 composite as shown in **Table 2** and **Table 3** respectively. This is probably because at 15 wt% there is not much thermoelectric particles, thus the x-rays may have passed through the gaps between the RCF strands hence recording a smaller crystallite size. However, from 30 wt% there is an increased packing of Bi_2Te_3 and Bi_2S_3 particles in the thermoelectric composite thus resulting in a slightly larger crystallite size.

In addition to the crystallite size, there is also a small decrease in the FWHM indicating improved crystallinity with the increasing incorporation of Bi_2Te_3 and Bi_2S_3 particles as shown in **Table 2** and **Table 3** respectively.

A lower microstrain and dislocation density is commonly preferred in order to lower electrical resistivity values (Grasso et al., 2013; Jariwala et al., 2015). With increasing Bi_2Te_3 and Bi_2S_3 concentration, the microstrain and dislocation density is seen to have decreased from 15 wt% to 45 wt% for RCF-Bi_2Te_3 composite and from 15 wt% to 30 wt% for RCF-Bi_2S_3 composite as shown in **Table 2** and **Table 3** respectively. The decreased microstrain and dislocation density is because Bi_2Te_3 and Bi_2S_3 particles filled in the gaps between RCF strands, which also led to a decrease in electrical resistivity as shown in **Figure 2**. Beyond 45 wt%, the increased packing of Bi_2Te_3 particles results in the propagation of small micro cracks on the surface of the RCF-Bi_2Te_3 composite that may have resulted in increased dislocation density and microstrain with a corresponding increase in electrical resistivity at 60 wt%.

On the other hand, for RCF-Bi_2S_3 composite, an increased dislocation density and microstrain was observed at 45 wt%, which also reflected on the increased electrical resistivity as shown in **Figure 2**. There is still a continuity between the RCF strands and polymer-Bi_2S_3 coating as shown in **Figure 6 (c)** thus still improving the power factors of the composite at 45 wt%. However, at 60 wt% there was a significant increase in microstrain and dislocation density even higher than 15 wt%, due to the discontinuity that occurred owing to the separation of the polymeric phase from the Bi_2S_3 particles as shown in **Figure 6 (d)**. Thus leading to a significant increase in electrical resistivity and drop in power factor at 60 wt%.

Table 2: FWHM, crystallite size, microstrain and dislocation density of RCF-Bi_2Te_3 composite.

Bi_2Te_3 Concentrations (wt%)	FWHM (radian)	Crystallite size, D (nm)	Microstrain (ε x 10^{-3}) ($lines^{-2}\ m^{-4}$)	Dislocation density (δ x 10^{14}) ($lines/m^2$)
15	0.0032	44.46	3.2	5.06
30	0.0031	46.74	3.1	4.58
45	0.0030	47.01	3.1	4.52
60	0.0031	45.69	3.2	4.79

Table 3: FWHM, crystallite size, microstrain and dislocation density of RCF-Bi_2S_3 composite.

Bi_2S_3 Concentrations (wt%)	FWHM (radian)	Crystallite size, D (nm)	Microstrain (ε x 10^{-3}) ($lines^{-2}\ m^{-4}$)	Dislocation density (δ x 10^{14}) ($lines/m^2$)
15	0.0031	45.69	3.50	4.79
30	0.0026	53.86	2.97	3.45
45	0.0027	52.14	3.08	3.68
60	0.0034	41.07	3.90	5.93

3.4. Thermal stability of RCF-Bi_2Te_3 and RCF-Bi_2S_3 composites

The thermal stabilities of both RCF-Bi_2Te_3 and RCF-Bi_2S_3 were evaluated using thermogravimetric analysis (TGA) and derivative thermogravimetric (DTG) studies. As thermoelectric composites are subjected to temperature differences, it is vital to determine the temperature range in which it is thermally stable.

The thermal stability of each constituent within the RCF-Bi_2Te_3 and RCF-Bi_2S_3 composite such as RCF, Bi_2Te_3, Bi_2S_3 and binder in the air are shown in **Figure S.6** (see Supplementary data). The polymeric binder experienced major degradation after 180 °C owing to the decomposition of some polyester components such as CO, CO_2, CH_4, ethylene and acetylene (Khalfallah et al., 2014). The RCF started to decompose from 260 °C, owing to residual epoxy that may still be present on its strands from previous applications. Bi_2Te_3 particles exhibited a thermally stable behaviour until 400 °C, beyond 400 °C the particles experienced oxidation that results in a sharp weight gain as shown in **Figure S.6** (see Supplementary

460 data). This weight gain was also observed by Brostow et al., that attributed it to the escape of
461 tellurium due to its low vapour pressure and subsequent oxidation of bismuth at 400 °C
462 (Brostow et al., 2012). On the other hand, Bi_2S_3 particles exhibited a thermally stable
463 behaviour in air as depicted in **Figure S.6** (see Supplementary data) until 530 °C, beyond that
464 it experienced a slight oxidation (540 °C) (due to the oxidation of its main constituents such
465 as Bi and Bi_2S_3 in the presence of oxygen in air (Rincbn, 1996), a subsequent mass
466 degradation (from 600 °C to 800 °C) and oxidized (beyond 800 °C).

467 Based on **Figure 9**, increasing amounts of Bi_2Te_3 and Bi_2S_3 had no significant change on the
468 T_{onset}. For RCF-Bi_2Te_3 composites, T_{onset} varied slightly from 308.46 °C (at lower loadings of
469 Bi_2Te_3) to 316.2 °C (at higher loadings of Bi_2Te_3). A similar pattern in the TGA analysis was
470 also observed for RCF-Bi_2S_3 composites until 45 wt% as shown in **Figure 9**. The T_{onset} varied
471 from 306.13 °C to 316.82 °C, at 60 wt% there is a slight drop in T_{onset} to 308.86 °C. At 60
472 wt%, due to high filler loading resulting in the separation of the polymer from the
473 thermoelectric fillers, may have resulted in lower thermal stabilities. All RCF-Bi_2Te_3 and
474 RCF-Bi_2S_3 composites started degrading at around 294 °C as shown in **Figure 9**. The
475 residual char was also seen to increase with increasing concentration of Bi_2Te_3 and Bi_2S_3
476 within the thermoelectric composite.

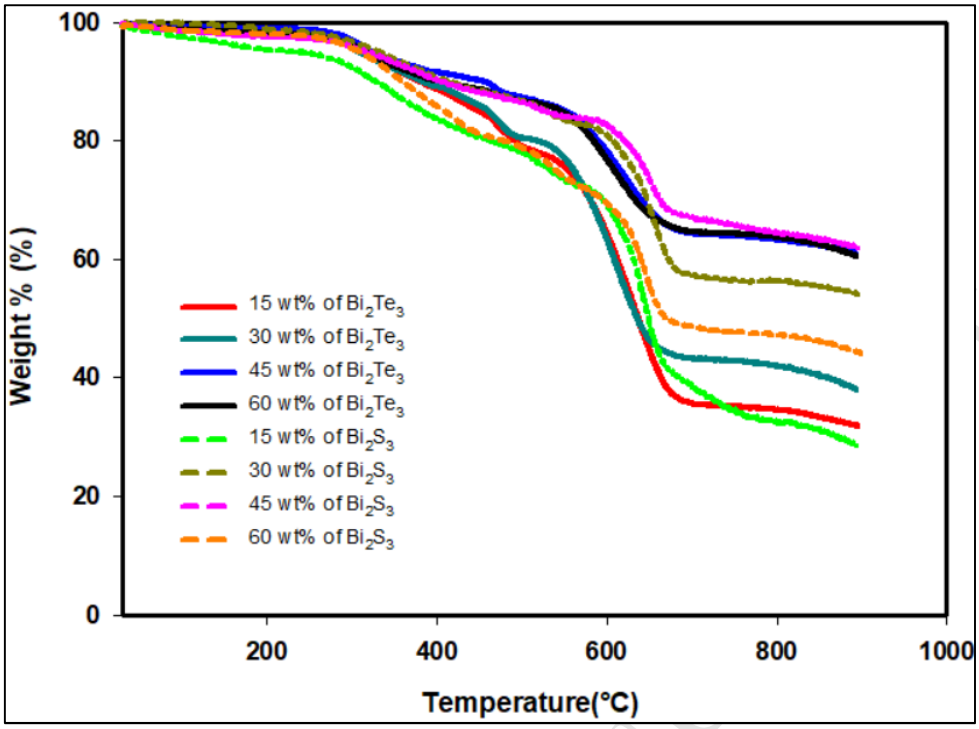

Figure 9: TGA analysis of RCF-Bi_2Te_3 and RCF-Bi_2S_3 composites.

Figure S.7 (see Supplementary data) shows the DTG curve of all the constituents in the RCF-Bi_2Te_3 and RCF-Bi_2S_3 composites. It can be seen that both RCF and binder started degrading at lower temperatures around 250 °C due to the lower thermal stability of polymeric compounds. On the other hand, both the thermoelectric fillers only exhibited degradation after 400 °C and 480 °C for Bi_2Te_3 and Bi_2S_3 respectively. The mass loss rate of the RCF and binder is higher than that of the thermoelectric fillers.

T_{max} is approximately 600 °C and 630 °C for all RCF-Bi_2Te_3 composites and RCF-Bi_2S_3 composites as shown in **Figure 10**. There was insignificant improvement in T_{max} with respect to increasing concentration of Bi_2Te_3 and Bi_2S_3. However, the mass loss rate of composites was reduced with increasing amount of Bi_2Te_3 and Bi_2S_3 and reached the least mass loss at 45 wt% thermoelectric filler loading. At concentrations higher than 45 wt%, there was no improvement in terms of mass loss rate for RCF-Bi_2Te_3 composites but however for RCF-Bi_2S_3 composites at 60 wt%, the mass loss rate was accelerated showing that it becomes less

thermally unstable than 45 wt%, which is also reflected on its decreased power factor as shown in **Figure 4**.

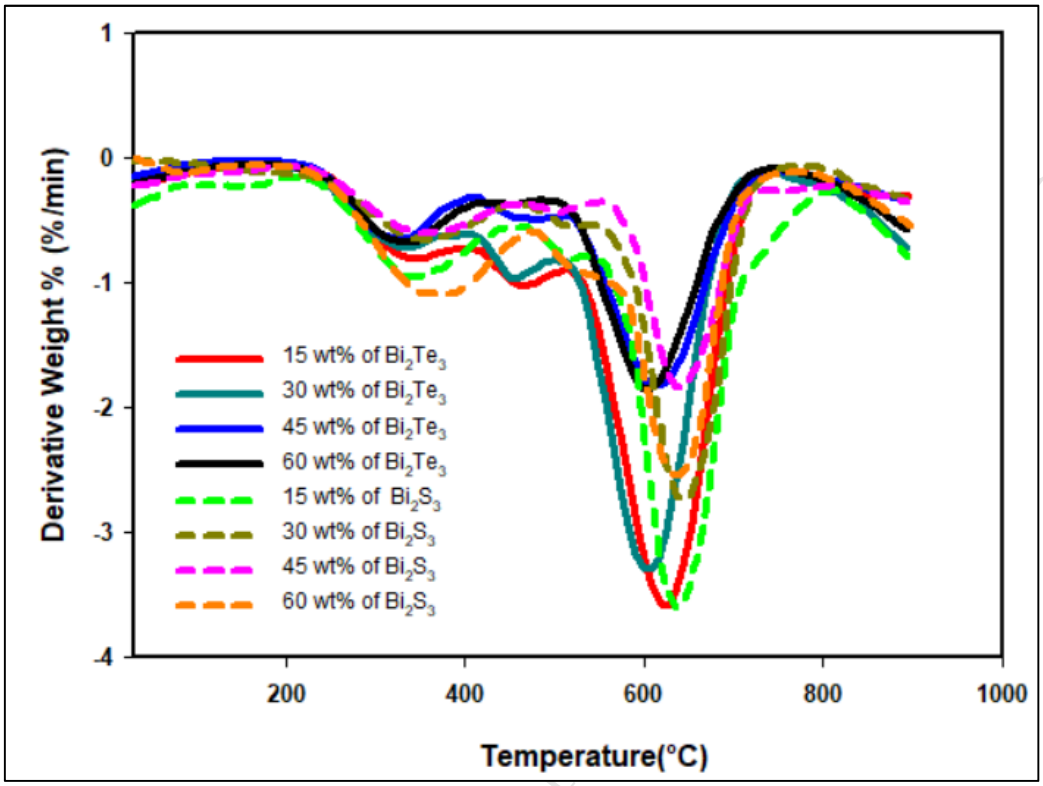

Figure 10: DTG curves of RCF-Bi_2Te_3 and RCF-Bi_2S_3 composites.

4. Conclusion

The power factor of RCF composite improved by 34 and 17 times upon the incorporation of thermoelectric fillers (Bi_2Te_3 and Bi_2S_3) respectively. The power factor of RCF composites increased with respect to increasing concentrations of Bi_2Te_3 and Bi_2S_3, however, it reached a maximum of $0.194 \pm 9.70\times10^{-3}$ $\mu WK^{-2}m^{-1}$ and $0.0941 \pm 4.71\times10^{-3}$ $\mu WK^{-2}m^{-1}$ for RCF-Bi_2Te_3 and RCF-Bi_2S_3 at 45 wt% respectively. The thermoelectric properties of both RCF-Bi_2Te_3 and RCF-Bi_2S_3 were remarkably higher than that of bare RCF as proved by the Seebeck coefficient, electrical resistivity, carrier property measurement, FESEM, EDX, XRD and TGA analysis. This is because the presence of the thermoelectric fillers not only suppressed

the carrier concentration but also improved the carrier mobility between the gaps of RCF strands, thus enhancing its thermoelectric capabilities.

The environmentally friendly Bi_2S_3 filler is seen to show promising thermoelectric properties, although it is one order lower than that of Bi_2Te_3 due to its innate material property that has high electrical resistivity. The thermoelectric composites are proven to be a cost effective and feasible alternative to producing efficient thermoelectric materials, which is economically efficient as well as industrially scalable with minimal infrastructure requirement. The proposed RCF composites in this study could be used for the recovery of low grade waste heat such as that from laptops and mobile devices to power low consumption electronic devices.

5. References

Brostow, W., Datashvili, T., Hagg Lobland, H.E., Hilbig, T., Su, L., Vinado, C., White, J., 2012. Bismuth telluride-based thermoelectric materials: Coatings as protection against thermal cycling effects. J. Mater. Res. 27, 2930–2936. https://doi.org/10.1557/jmr.2012.335

Cholake, S.T., Moran, G., Joe, B., Bai, Y., Singh Raman, R.K., Zhao, X.L., Rizkalla, S., Bandyopadhyay, S., 2016. Improved Mode I fracture resistance of CFRP composites by reinforcing epoxy matrix with recycled short milled carbon fibre. Constr. Build. Mater. 111, 399–407. https://doi.org/10.1016/j.conbuildmat.2016.02.039

Du, X., Cai, F., Wang, X., 2014. Enhanced thermoelectric performance of chloride doped bismuth sulfide prepared by mechanical alloying and spark plasma sintering. J. Alloys Compd. 587, 6–9. https://doi.org/10.1016/j.jallcom.2013.10.185

F.Keuch, T., 2015. Thin Films and Epitaxy: Basic Techniques, and Materials, Processes, and Technology. Elsevier, Oxford.

Feng, N., Wang, X., Wu, D., 2013. Surface modification of recycled carbon fiber and its reinforcement effect on nylon 6 composites: Mechanical properties, morphology and crystallization behaviors. Curr. Appl. Phys. 13, 2038–2050. https://doi.org/10.1016/j.cap.2013.09.009

Fernández-Yáñez, P., Gómez, A., García-Contreras, R., Armas, O., 2018. Evaluating thermoelectric modules in diesel exhaust systems: potential under urban and extra-urban driving conditions. J. Clean. Prod. 182, 1070–1079. https://doi.org/https://doi.org/10.1016/j.jclepro.2018.02.006

539 Grasso, S., Tsujii, N., Jiang, Q., Khaliq, J., Maruyama, S., Miranda, M., Simpson, K., Mori,
540 T., Reece, M.J., 2013. Ultra low thermal conductivity of disordered layered p-type
541 bismuth telluride. J. Mater. Chem. C 1, 2362. https://doi.org/10.1039/c3tc30152d

542 Hambach, M., Möller, H., Neumann, T., Volkmer, D., 2016. Carbon fibre reinforced cement-
543 based composites as smart floor heating materials. Compos. Part B Eng. 90, 465–470.
544 https://doi.org/http://dx.doi.org/10.1016/j.compositesb.2016.01.043

545 Hasan, B.A., Shallal, I.H., 2014. Structural and Optical Properties of SnS Thin Films. J.
546 Nanotechnol. Adv. Mater. 2, 43–49. https://doi.org/10.1080/17458080.2013.788226

547 Howarth, J., Mareddy, S.S.R., Mativenga, P.T., 2014. Energy intensity and environmental
548 analysis of mechanical recycling of carbon fibre composite. J. Clean. Prod. 81, 46–50.
549 https://doi.org/https://doi.org/10.1016/j.jclepro.2014.06.023

550 Jagadish, P.R., Khalid, M., Amin, N., Li, L.P., Chan, A., 2017. Process optimisation for n-
551 type Bi2Te3 films electrodeposited on flexible recycled carbon fibre using response
552 surface methodology. J. Mater. Sci. 52, 11467–11481. https://doi.org/10.1007/s10853-
553 017-1284-2

554 Jagadish, P.R., Li, L.P., Chan, A., Khalid, M., 2016. Effect of Annealing on Virgin and
555 Recycled Carbon Fiber Electrochemically Deposited with N-type Bismuth Telluride and
556 Bismuth Sulfide. Mater. Manuf. Process. 31, 1223–1231.
557 https://doi.org/10.1080/10426914.2015.1090590

558 Jariwala, B., Shah, D., Ravindra, N.M., 2015. Influence of doping on structural and optical
559 properties of Bi 2 Te 3 thin films. Thin Solid Films 589, 396–402.
560 https://doi.org/10.1016/j.tsf.2015.05.020

561 Khalfallah, M., Abbès, B., Abbès, F., Guo, Y.Q., Marcel, V., Duval, A., Vanfleteren, F.,
562 Rousseau, F., 2014. Innovative flax tapes reinforced Acrodur biocomposites: A new
563 alternative for automotive applications. Mater. Des. 64, 116–126.
564 https://doi.org/10.1016/j.matdes.2014.07.029

565 Kim, M.Y., Oh, T.S., 2009. Electrodeposition and thermoelectric characteristics of Bi 2Te 3
566 and Sb 2Te 3 films for thermopile sensor applications. J. Electron. Mater. 38, 1176–
567 1181. https://doi.org/10.1007/s11664-008-0653-7

568 Kioupakis, E., Tiago, M.L., Louie, S.G., 2010. Quasiparticle electronic structure of bismuth
569 telluride in the GW approximation. Phys. Rev. B - Condens. Matter Mater. Phys. 82, 1–
570 4. https://doi.org/10.1103/PhysRevB.82.245203

571 Kishita, Y., Ohishi, Y., Uwasu, M., Kuroda, M., Takeda, H., Hara, K., 2016. Evaluating the
572 life cycle CO2 emissions and costs of thermoelectric generators for passenger
573 automobiles: a scenario analysis. J. Clean. Prod. 126, 607–619.
574 https://doi.org/https://doi.org/10.1016/j.jclepro.2016.02.121

575 Kusagaya, K., Takashiri, M., 2015. Investigation of the effects of compressive and tensile
576 strain on n-type bismuth telluride and p-type antimony telluride nanocrystalline thin
577 films for use in flexible thermoelectric generators. J. Alloys Compd. 653, 480–485.
578 https://doi.org/10.1016/j.jallcom.2015.09.039

579 Li, D., Sun, R.R., Qin, X.Y., 2011. Improving thermoelectric properties of p-type Bi2Te3-
580 based alloys by spark plasma sintering. Prog. Nat. Sci. Mater. Int. 21, 336–340.
581 https://doi.org/10.1016/S1002-0071(12)60066-5

582 Li, M., Li, S., Liu, J., Wen, X., Tang, T., 2016. Striking effect of epoxy resin on improving
583 mechanical properties of poly(butylene terephthalate)/recycled carbon fibre composites.
584 Compos. Sci. Technol. 125, 9–16. https://doi.org/10.1016/j.compscitech.2016.01.015

585 Li, X., Bai, R., McKechnie, J., 2016. Environmental and financial performance of mechanical
586 recycling of carbon fibre reinforced polymers and comparison with conventional
587 disposal routes. J. Clean. Prod. 127, 451–460.
588 https://doi.org/https://doi.org/10.1016/j.jclepro.2016.03.139

589 Liufu, S.C., Chen, L.D., Yao, Q., Wang, C.F., 2007. Assembly of one-dimensional nanorods
590 into Bi2S3 films with enhanced thermoelectric transport properties. Appl. Phys. Lett. 90,
591 1–4. https://doi.org/10.1063/1.2712504

592 Marsh, G., 2014. Composites flying high. Reinf. Plast. 58, 14–18.
593 https://doi.org/10.1016/S0034-3617(14)70133-X

594 Marsh, G., 2009. Carbon recycling: a soluble problem. Reinf. Plast. 53, 22-23-27.
595 https://doi.org/10.1016/S0034-3617(09)70149-3

596 McConnell, V.P., 2010. Launching the carbon fibre recycling industry. Reinf. Plast. 54, 33–
597 37. https://doi.org/10.1016/S0034-3617(10)70063-1

598 Pang, E.J.X., Pickering, S.J., Chan, a., Wong, K.H., Lau, P.L., 2012. N-type thermoelectric
599 recycled carbon fibre sheet with electrochemically deposited Bi2Te3. J. Solid State
600 Chem. 193, 147–153. https://doi.org/10.1016/j.jssc.2012.04.046

601 Rahman, A.A.A., Ali Umar, A., Othman, M.H.U., 2015. Effect of bismuth telluride
602 concentration on the thermoelectric properties of PEDOT:PSS-glycerol organic films.
603 Phys. E Low-Dimensional Syst. Nanostructures 66, 293–298.
604 https://doi.org/10.1016/j.physe.2014.10.032

605 Rincbn, M.E., 1996. Kinetics of electrical conductivity enhancement in bismuth sulphide thin
606 films . Part ii : optoelectronic properties (film) and phase transformations (powder)
607 under oxygen annealing 57, 1947–1955.

608 Rowe, D., 1995. Introduction, in: CRC Handbook of Thermoelectrics. CRC Press.
609 https://doi.org/doi:10.1201/9781420049718.ch1

610 Shuaib, N.A., Mativenga, P.T., 2016. Energy demand in mechanical recycling of glass fibre
611 reinforced thermoset plastic composites. J. Clean. Prod. 120, 198–206.
612 https://doi.org/10.1016/j.jclepro.2016.01.070

613 Tian, X., Liu, T., Wang, Q., Dilmurat, A., Li, D., Ziegmann, G., 2017. Recycling and
614 remanufacturing of 3D printed continuous carbon fiber reinforced PLA composites. J.
615 Clean. Prod. 142, 1609–1618.
616 https://doi.org/https://doi.org/10.1016/j.jclepro.2016.11.139

617 Timmis, A.J., Hodzic, A., Koh, L., Bonner, M., Soutis, C., Sch??fer, A.W., Dray, L., 2015.
618 Environmental impact assessment of aviation emission reduction through the
619 implementation of composite materials. Int. J. Life Cycle Assess. 20, 233–243.
620 https://doi.org/10.1007/s11367-014-0824-0

621 Tsukamoto, J., Takahashi, A., Tani, T., Ishiguro, T., 1989. Thermoelectric power of heat-
622 treated CVD carbon fibers. Carbon N. Y. 27, 919–923. https://doi.org/10.1016/0008-
623 6223(89)90042-0

624 Venkatasubramanian, R., Siivola, E., Colpitts, T., O'quinn, B., 2001. Thin-film
625 thermoelectric devices with high room-temperature figures of merit. Nature 597–602.

626 Wang, D., Su, Y., Chen, D., Wang, L., Xiang, X., Zhu, D., 2015. Preparation and
627 characterization of poly(3-octylthiophene)/carbon fiber thermoelectric composite
628 materials. Compos. Part B Eng. 69, 467–471.
629 https://doi.org/10.1016/j.compositesb.2014.10.007

630 Wong, D.P., Chien, W.-L., Huang, C.-Y., Chang, C., Ganguly, A., Lyu, L.-M., Hwang, J.-S.,
631 Chen, L.-C., Chen, K.-H., 2016. Enhanced thermoelectric performance in a percolated
632 bismuth sulfide composite. RSC Adv. 6, 98952–98955.
633 https://doi.org/10.1039/C6RA21418E

634 Wong, K.H., Pickering, S.J., Rudd, C.D., 2010. Recycled carbon fibre reinforced polymer
635 composite for electromagnetic interference shielding. Compos. Part A Appl. Sci. Manuf.
636 41, 693–702. https://doi.org/10.1016/j.compositesa.2010.01.012

637 Yu, Y.Q., Zhang, B.P., Ge, Z.H., Shang, P.P., Chen, Y.X., 2011. Thermoelectric properties of
638 Ag-doped bismuth sulfide polycrystals prepared by mechanical alloying and spark
639 plasma sintering. Mater. Chem. Phys. 131, 216–222.
640 https://doi.org/10.1016/j.matchemphys.2011.09.010

641 Yücel, E., Yücel, Y., 2017a. Fabrication and characterization of Sr-doped PbS thin films
642 grown by CBD. Ceram. Int. 43, 407–413.
643 https://doi.org/10.1016/j.ceramint.2016.09.173

644 Yücel, E., Yücel, Y., 2017b. Effect of doping concentration on the structural, morphological
645 and optical properties of Ca-doped PbS thin films grown by CBD. Opt. - Int. J. Light
646 Electron Opt. 142, 82–89. https://doi.org/https://doi.org/10.1016/j.ijleo.2017.04.104

647 Zhao, L.-D., Zhang, B.-P., Liu, W.-S., Zhang, H.-L., Li, J.-F., 2008. Enhanced thermoelectric
648 properties of bismuth sulfide polycrystals prepared by mechanical alloying and spark
649 plasma sintering. J. Solid State Chem. 181, 3278–3282.
650 https://doi.org/10.1016/j.jssc.2008.08.022

651

Highlights

- Reuse of recycled carbon fibre (RCF) for thermoelectric applications.
- Power factor improved by 34 and 17 times upon incorporation of Bi_2Te_3 and Bi_2S_3.
- Highest power factor at 45 wt% of thermoelectric filler loading.
- Attained power factor of 0.194 $\mu WK^{-2}m^{-1}$ (Bi_2Te_3) and 0.0941 $\mu WK^{-2}m^{-1}$ (Bi_2S_3).
- Thermoelectric composites at all concentrations are thermally stable until 294 °C.